

To appear in the *Journal of Geophysical Research*, 2000.

A non-linear optimal estimation inverse method for radio occultation measurements of temperature, humidity and surface pressure

Paul I. Palmer¹, J. J. Barnett

Department of Physics, Clarendon Laboratory, Oxford, United Kingdom

J. R. Eyre, S. B. Healy

Satellite Applications Division, United Kingdom Meteorological Office, Bracknell, United Kingdom

Abstract

An optimal estimation inverse method is presented which can be used to retrieve simultaneously vertical profiles of temperature and specific humidity, in addition to surface pressure, from satellite-to-satellite radio occultation observations of the Earth's atmosphere. The method is a non-linear, maximum *a posteriori* technique which can accommodate most aspects of the real radio occultation problem and is found to be stable and to converge rapidly in most cases. The optimal estimation inverse method has two distinct advantages over the analytic inverse method in that it accounts for some of the effects of horizontal gradients and is able to retrieve optimally temperature and humidity simultaneously from the observations. It is also able to account for observation noise and other sources of error. Combined, these advantages ensure a realistic retrieval of atmospheric quantities.

A complete error analysis emerges naturally from the optimal estimation theory, allowing a full characterisation of the solution. Using this analysis a quality control scheme is implemented which allows anomalous retrieval conditions to be recognised and removed, thus preventing gross retrieval errors.

The inverse method presented in this paper has been implemented for bending angle measurements derived from GPS/MET radio occultation observations of the Earth. Preliminary results from simulated data suggest that these observations have the potential to improve NWP model analyses significantly throughout their vertical range.

1. Introduction

Radio occultation (RO) experiments have played a prominent role in the NASA programme for solar system exploration for more than two decades and have contributed to studies of the atmosphere of Mars [Fjeldbo and Eshleman, 1968], Venus [Fjeldbo and Kliore, 1971], Jupiter [Kliore et al, 1975], Saturn [Lindal et al, 1985], Uranus [Lindal et al, 1987], and Neptune [Lindal 1992]. This method of radio occultation uses a receiver on Earth and a satellite occulted by a planetary atmosphere (which may occur from either a fly-by or by a satellite orbit of the planet). Suitably accurate atmospheric RO measurements of the Earth’s atmosphere became possible with the advent of the Global Positioning System (GPS), but it was not until the late 1980s–early 1990s that the potential of RO using the GPS was widely appreciated (e.g. Gurvich and Krasil’nikova, [1990]).

The radio occultation method used to sound the Earth’s atmosphere is different from that used by the planetary experiments, in that both the receiver and the transmitters are orbiting the planet.

Data from the prototype GPS space-borne receiver, GPS/MET, launched in April 1995, confirmed the potential of obtaining accurate, global observations of the Earth’s atmosphere from the radio occultation technique. Temperature comparisons between early results from the GPS/MET receiver and collocated radiosondes and numerical weather prediction (NWP) model analyses showed good agreement (e.g. Kursinski et al, [1996]; Ware et al, [1996]).

The analytic method of inverting radio occultation measurements to obtain meteorological parameters (i.e. the method used to sound other planetary atmospheres) involves the use of an integral transform, using the assumption of a horizontally homogeneous atmosphere, to obtain a profile of refractivity (as a function of geometric height) [Fjeldbo and Eshleman, 1968]. The hydrostatic relation is used to obtain pressure and temperature from refractivity via density. For the Earth’s atmosphere, where a reasonable prior knowledge of horizontal gradients is available, the analytic inversion does not represent the most suitable method since inadequate modelling of such gradients can cause large retrieval errors (e.g. Ahmad and Tyler, [1998]).

Eyre, [1994] addresses this issue and suggests a statistically optimal retrieval approach, using variational methods, to enable the direct assimilation of bending angle or refractivity (Healy and Eyre, [1999] investi-

gate the latter quantity). Zou et al, [1995] also looked at the impact of atmospheric radio refractivity measurements using a 4-D variational data assimilation approach. Their results showed that the measurements were effective in recovering the vertical profiles of water vapour, and found that the accuracy of the derived water vapour field was significantly better than that obtained through the analytic retrieval technique. The assimilation of these measurements were also shown to provide useful temperature information. There have also been several numerical experiments which have assessed simulated GPS/MET refractivity measurements to predict cyclonic disturbances (e.g. Kuo et al, [1998]), and have concluded that these measurements are likely to have a significant impact on short-range operational NWP, with the caveat that the number of GPS receivers will have to be increased before the full potential impact of this measurement could be realised.

In this paper we utilise a non-linear optimal estimation technique which is implemented and validated using an ensemble of simulated retrieval scenarios, using the bending angle quantity as the ‘observation’.

Section 2 outlines the details of the RO methodology for the Earth’s atmosphere necessary to derive the bending angle quantity, recalls the analytic inverse method and discusses the impetus for pursuing an alternative inverse method. In section 3 we outline the theory for the non-linear optimal estimation inverse method and give details of its implementation for GPS RO observations. Section 4 is devoted to details of the validation of the optimal estimation inverse method with reference to GPS RO observations. The sensitivity of the inverse model assumptions is also investigated, and we conclude the paper with a discussion of the results obtained.

2. Radio occultation measurements of Earth’s atmosphere

Kursinski et al, [1997] give a detailed description of the method used to measure the RO atmospheric observables; the following section gives a summary of the theory, assuming no external encryption of the signals.

The GPS satellites transmit on two L-band radio frequencies¹. Assuming a continuous link between the receiver and transmitter, when the receiver passes behind the atmosphere with respect to a GPS transmit-

¹Namely, L1: 1.57542 GHz and L2: 1.2272 GHz.

ter the signal travels through the atmosphere and is refracted in response to variations of refractive index along its path. This refraction causes the ray to travel over a longer path than it would in the absence of the atmosphere, in accordance with Fermat's principle of least time, which subsequently causes an atmospheric time delay in the received signal.

The Doppler shift of the signal is calculated from the additional atmospheric delay (the derivative of the phase delay). Using the geometry and notation of figure 1, the Doppler shift f_d of the carrier frequency f_0 measured by the receiver is given by:

$$f_d = f_0 \left[\frac{(\mathbf{v}_T \cdot \mathbf{n}_T + \mathbf{v}_R \cdot \mathbf{n}_R)}{c} \right] \quad (1)$$

where $\mathbf{v}_{T,R}$ are transmitter and receiver velocity vectors, $\mathbf{n}_{T,R}$ are path direction vectors of the transmitter and receiver, and c is the velocity of light.

There are also relativistic terms which need to be considered in equation 1 (due to different gravitational potentials and higher order corrections for spacecraft velocity) but these can be eliminated based on knowledge of orbital geometry and the Earth's gravity field [Kursinski *et al.*, 1997]. Note that the relative positions and velocities of the two satellites can be calculated very accurately using available tracking data, which is independent of radio occultation data.

By specifying radial and tangential components of the velocity of satellite i in the plane coinciding with the ray trajectory as \mathbf{v}_i^r and \mathbf{v}_i^t , and taking into account Snell's law, the angles ϕ_R and ϕ_T can be calculated from the following relations:

$$f_d = f_0 c^{-1} (\mathbf{v}_R^r \cos \phi_R + \mathbf{v}_T^r \cos \phi_T + \mathbf{v}_R^t \sin \phi_R - \mathbf{v}_T^t \sin \phi_T) \quad (2)$$

The cumulative effect of the atmosphere on the ray path can be expressed in terms of the total refractive bending angle, ε , as a function of the impact parameter, a . The impact parameter may be defined as the perpendicular distance between the local curvature of the Earth at the tangent point of the ray and the asymptotic straight line followed by the ray as it approaches the atmosphere.

From Bouguer's rule [Born and Wolf, 1993], and the geometry defined by figure 1, $\varepsilon(a)$ can be calculated thus

$$r_R \sin \phi_R = r_T \sin \phi_T = a \quad (3)$$

$$\varepsilon = \phi_R + \phi_T + \theta - \pi \quad (4)$$

It is this rule that introduces the assumption of spherical symmetry ($nr \sin \phi = a$, where a is a constant along the ray path), i.e. a horizontally homogeneous atmosphere. Departures from this assumption can introduce significant errors if not properly accounted for. These errors have been studied by Ahmad and Tyler, [1999] and Healy, [1999], but are not addressed in the study presented here.

Measurements of the time delay become possible for neutral atmospheric sounding when the GPS signal begins to transect the mesosphere at an altitude of about 85 km; at this altitude the atmospheric phase delay is about 1 mm (3×10^{-12} s) which can be observed by the LEO GPS receiver [Ware *et al.*, 1996]. Further information about the measurement characteristics may be obtained from Kursinski *et al.*, [1997].

2.1. The analytic inverse method

Using an Abel integral transform (equation 5), or making use of a similar integral transform when applying Fresnel diffraction theory [Mortensen and Høeg, 1998], these bending angle measurements can be inverted to obtain a profile of refractivity. For completeness sake, the 'forward' Abel integral transform (equation 6) is presented alongside the 'inverse' Abel integral transform:

$$\ln n(x) = \frac{1}{\pi} \int_x^{+\infty} \varepsilon(a) (a^2 - x^2)^{-1/2} da \quad (5)$$

$$\varepsilon(a) = -2a \int_a^{+\infty} \left(\frac{\partial \ln n(x)}{\partial x} \right) (x^2 - a^2)^{-1/2} dx, \quad (6)$$

where n is the refractive index and x is the refractive radius (i.e. $x = rn$).

Geometric height levels, z , can be obtained from the refractive index profile, as a function of impact parameter, and the local radius of curvature, R_c , thus

$$z = \frac{x}{n} - R_c. \quad (7)$$

Because refractive index is near unity, refractivity N is used to describe the refractive medium which is given by $N = (n - 1) \times 10^6$.

Refractivity is affected primarily by air density (dependent on pressure and temperature) and water vapour density, thus the measurement contains information about both. Equation 8 describes this relationship,

$$N = \frac{c_1 P_a}{T} + \frac{c_2 P_W}{T^2} \quad (8)$$

where P_a is the total atmospheric pressure (hPa), P_W is the partial pressure of water vapour, T is the temperature (K), and c_1 and c_2 represent constants of proportionality, whose values are $77.6 \text{ (KhPa}^{-1}\text{)}$ and $3.73 \times 10^5 \text{ (K}^2\text{hPa}^{-1}\text{)}$, respectively. The form of the dry and moist terms in equation 8 is from *Smith and Weintraub*, [1953].

Refractivity is also affected by charged particles in the ionosphere and the scattering by water droplets suspended in the atmosphere. The first-order ionospheric contribution to refractivity can be removed by combining the two GPS signals (described by *Vorob'ev and Krasil'nikova*, [1997]), leaving higher-order terms, and the scattering contribution is found to be negligible compared to the contribution due to air and water vapour density [*Kursinski et al*, 1997].

There is no measurement information to allow the separation of the effects of temperature and water vapour, and therefore these quantities can be retrieved only using prior information. If the absolute humidity is judged to be small (e.g. in the coldest regions of the troposphere and stratosphere, with temperatures less than 250 K), it may be neglected, and density calculated from refractivity. The hydrostatic relation can be used to calculate values of pressure, and hence temperature. However, if humidity is judged to be significant, then an iterative process may be used to calculate temperature/humidity if an *a priori* profile of humidity/temperature is used. This prior information can be taken from various sources such as collocated NWP model output.

The inability of this inverse method to account for horizontal refractivity inhomogeneities, and the sub-optimal way this method retrieves temperature and humidity with prior values, represents two key disadvantages of this method, and form part of the impetus to develop a new inverse method.

The hydrostatic relation, used to compute values of pressure on the retrieved height levels, requires an assumed pressure value at a particular geometric height level. A variety of methods have been implemented to tackle this initial value problem. *Kursinski et al*, [1996] assumed a temperature of 260 K at 50 km. This method has the problem that if the assumed temperature is inconsistent with the measurements an error is introduced, which decreases exponentially with depth. More elaborate methods (e.g. *Rocken et al*, [1997] and *Steiner et al*, [1999]) initialise

the GPS/MET retrieval at some high altitude (e.g. 100 km) using climate model data, and combine the measurements and model data to minimise downward propagation of errors. In principle, the method presented in this paper also combines the model data and the observations but achieves this is an optimal way. The method presented also has the advantage of a straightforward error characterisation.

Since GPS RO observations sometimes reach near-surface altitudes (i.e. less than 1 km from the surface), surface pressure is also retrieved using the optimal estimation inverse method.

3. The optimal estimation inverse method

The method outlined here is also known as one-dimensional variational data analysis.

The main advantage of this method is that it provides simultaneous estimates of temperature and humidity profiles that are statistically optimal, given prior estimates from an NWP model (together with their error covariances). It also provides a framework for assessing the error characteristics of the estimates.

In this study only the 1-d problem has been studied. However, the errors introduced by the neglect of the horizontal gradients have been estimated and allowed for as part of the error budget (see section 3.2 “Forward modelling errors”).

3.1. Theory

A brief description of the theory used in optimal estimation is presented here; a more detailed description may be found in *Rodgers*, [1976] and *Rodgers*, [1990].

For brevity, the observation noise, the error associated with any forward modelling parameters and the forward model error (which includes the representativeness error [*Lorenc*, 1986]) will be accounted for in one vector which will be denoted by ϵ and its ensemble characteristics described by the covariance matrix \mathbf{E} .

The rationale behind optimal estimation is to minimise a cost functional $\mathbf{J}(\mathbf{x})$ (or to solve $\nabla_{\mathbf{x}}\mathbf{J}(\mathbf{x})=0$), which measures the degree of fit of estimates of the atmospheric state to the measurements and to some prior information, and possibly to some other physical or dynamical constraints. In this case $\mathbf{J}(\mathbf{x})$ is given by

$$\mathbf{J}(\mathbf{x}) = (\mathbf{y}^o - \mathbf{y}(\mathbf{x}))^T \mathbf{E}^{-1} (\mathbf{y}^o - \mathbf{y}(\mathbf{x})) + (\mathbf{x} - \mathbf{x}^b)^T \mathbf{C}^{-1} (\mathbf{x} - \mathbf{x}^b) \quad (9)$$

where \mathbf{x}^b and \mathbf{x} represent the background and updated state vectors, respectively; \mathbf{y}^o and $\mathbf{y}(\mathbf{x})$ represent the observation vector and the estimated observation vector calculated from the state vector (*Eyre, [1994]*), respectively; and \mathbf{C} represents the background error covariance matrix.

There are a number of methods available to minimise $\mathbf{J}(\mathbf{x})$: the scheme described here uses the Levenberg-Marquardt iterative method [e.g. *Press et al, 1992*]:

$$\mathbf{x}_{i+1} = \mathbf{x}^b + ((1 + \gamma)\mathbf{C}^{-1} + \mathbf{K}^T \mathbf{E}^{-1} \mathbf{K})^{-1} [(\mathbf{K}^T \mathbf{E}^{-1} (\mathbf{y}^o - \mathbf{y}(\mathbf{x}_i))) + (\gamma \mathbf{C}^{-1} + \mathbf{K}^T \mathbf{E}^{-1} \mathbf{K})(\mathbf{x}_i - \mathbf{x}^b)] \quad (10)$$

where \mathbf{K} is $\nabla_{\mathbf{x}_i} \mathbf{y}(\mathbf{x}_i)$, γ is a non-dimensional weighting factor², and all other variables are as before.

Using the optimal estimation theory it is possible to obtain an error covariance for the retrieved products. Indeed, it can be argued that the retrieved products are of limited value without an estimate of their uncertainty. The solution error covariance $\hat{\mathbf{S}}$ is given approximately (i.e. at the linear limit) by

$$\hat{\mathbf{S}} = (\mathbf{C}^{-1} + \mathbf{K}^T \mathbf{E}^{-1} \mathbf{K})^{-1}. \quad (11)$$

The solution error covariance can then be compared with the prior error covariance to ascertain how the retrieval has improved upon the prior knowledge of the atmospheric state.

3.2. Implementation of the optimal estimation inverse model

This subsection describes in detail the components of equation 9.

The background state vector and its uncertainty covariance matrix In this case the background knowledge of the atmosphere state \mathbf{x}^b was obtained from short-range forecasts provided by the UKMO unified model [*Cullen, 1993*]. The model from which the data are derived had 19 levels, which were expressed on hybrid-sigma pressure coordinates

²for increasing values of γ this minimisation method degenerates into the method of steepest descent.

(surface–10 hPa). The global model had a resolution of 0.833° (180°/217) latitude and 1.25° (360°/288) longitude.

The data used are 6-hour forecasts which have been interpolated to occultation event positions, using the mean latitude and longitude of each occultation³.

These 19 levels are linearly interpolated (in ln-pressure) onto the state vector levels used for TOVS retrievals [*Eyre, 1990*]. CIRA climatology [*CIRA, 1986*] is assumed above the UKMO model accounting for the latitudinal and seasonal variation of the profile. This climatology provides a reasonable prior and first guess information in the upper stratosphere.

For the forecast error covariance matrix \mathbf{C} (described in *Eyre, [1989]*), lower atmospheric values (surface–50 hPa) were generated from radiosonde–forecast difference statistics and upper stratosphere values were found by regression from the levels provided [*Eyre, 1989*].

The radio occultation retrieval uses 40 temperature elements, 15 ln(specific humidity) elements⁴ and a surface pressure element from this forecast error covariance matrix. The temperature and ln(specific humidity) inter-quantity covariance values have been set to zero. These inter-quantity covariances are not well known and assuming zero covariance between them is more conservative than an erroneous covariance. The surface pressure element is uncorrelated with both temperature and ln(specific humidity).

Since CIRA climatology is used to form the *a priori* (and the first-guess) it is necessary to consider the errors that may be attached to such information. In general, if the standard deviation values from the diagonal elements of the forecast error covariance matrix are smaller than the uncertainties assumed for the climatology, then the climatological errors are used at the levels in the upper atmosphere described by the CIRA climatology (off-diagonal elements remain the same): at latitude θ , for $|\theta| \geq 45^\circ$ $\sigma=15$ K (winter) and $\sigma=5$ K (summer); and for $|\theta| \leq 45^\circ$ $\sigma=5$ K.

The values for the diagonal elements of the UKMO forecast error covariance matrix are shown by figure 2.

As expected for temperature, the lower atmosphere

³The mean latitude and longitude of an occultation corresponds typically to altitudes in the lower stratosphere/upper troposphere.

⁴Specific humidity is expressed as the natural logarithm of specific humidity since forecast errors in this quantity are more constant than in specific humidity.

forecast errors are reasonably small (of the order of 1.5 K) and increase as a function of altitude. The actual values have been developed over recent years at the UKMO and reflect the average error in six-hour forecasts.

The observation vector and its error covariance matrix The observation vector \mathbf{y}^o contains bending angle measurements as a function of impact parameter (section 2).

In practice, atmospheric phase delay measurements from the GPS/MET receiver are low-pass filtered to reduce noise. The cut-off frequency of the filter is tuned to pass phase variations corresponding to vertical scales of 2 to 3 km in the stratosphere and approximately 200 m in the lower troposphere [Rocken *et al.*, 1997]. From the phase observable, Doppler shifts (and subsequently bending angle profiles) for the two GPS signals are computed. First-order ionospheric effects are removed from the data by combining the two signals to form a single corrected profile [Vorob'ev and Krasil'nikova, 1994]. Typically, after filtering, there are 100–200 neutral atmosphere bending angle measurements, which span a vertical range of approximately 0.5–60 km.

In addition to the observation error covariance matrix consisting of observation noise estimates, errors from the forward modelling and forward model parameters are considered.

Observation noise Observation errors are created by the hardware of the measurement system and by the pre-processing of the observations. The observation noise estimates are taken from the work described in Luntama, [1997]. They include thermal noise, residual errors from the ionospheric correction, local multipath (distortions when the transmitted signal is reflected from a surface near the signal propagation path), orbit determination accuracy, and clock instabilities of low-Earth-orbit receiver and GPS satellites and ground stations.

These observation error estimates are based on phase noise levels during the measurement or estimated from other noise sources during a radio occultation event. The effect from satellite clock errors and from the selective availability military encryption process were found to be negligible by assuming a differencing decryption technique (involving the differencing of the several sets of signals, using the satellites and the ground stations) [Kursinski *et al.*, 1997]. The only exception is the residual error from the ionospheric correction which was obtained from refractivity error estimates published in Kursinski *et*

al., [1997] and mapped to bending angle space using a forward model [Luntama, 1997].

The observation error estimates⁵ used in the optimal estimation technique are shown by figure 3. These estimates represent normal atmospheric conditions with a relatively small multipath error (3 mm) and normal ionospheric conditions. Panel (a) shows that there are a number of noise contributions of comparable size in the lower atmosphere. At altitudes above 30 km the residual ionospheric correction error begins to dominate the total bending angle error curve (panel (b)).

These noise estimates are assumed to be fully independent, i.e. their inter-level (and inter-quantity) covariance is zero. However, the bending angle measurements do contain a small, local correlation between successive levels due to filtering of the phase measurements. Because this correlation is small, the diagonal form is a good approximation to the full matrix [J. P. Luntama: personal communication].

Real observations from the GPS/MET data used have been found to be noisier than theoretical estimates [Luntama, 1997]. Bending angle fluctuations in the upper stratosphere (of the order of 10^{-5} radians) are present and are thought to be due to residual errors from the LEO satellite clock calibration in the differencing decryption technique (see “Observation noise”) [Syndergaard, 1999]. As such, a suitable error is attached to reflect the upper atmosphere measurements.

Forward modelling errors In this work the forward model used to map from state space to observation space is described in Eyre, [1994] but applied to an atmosphere approximated as spherical symmetric about the given profile at the tangent point. Essentially the geophysical parameters are converted to refractivity as a function of height, and subsequently impact parameter using the local radius of curvature. The resulting profile is mapped into observation space using the ‘forward’ Abel integral transform (equation 6).

The two main forward modelling errors are due to the assumption of a horizontally homogeneous atmosphere and a representativeness error.

Estimates for the first of these errors are obtained using a version of the forward model which can ac-

⁵These estimates have been computed by a nominal bending angle profile defined using an exponential curve with a scale height of approximately 7 km [J. P. Luntama: personal communication].

count for horizontal inhomogeneities in the plane of the ray path (described in *Eyre*, [1994]) and comparing observation vectors with the version of the forward model which assumes a horizontal homogeneous atmosphere [*Palmer*, [1998]]. Mid-latitude two-dimensional NWP fields ($0-360^\circ$) were used to simulate typical horizontal gradients in temperature and humidity. By considering small sections of the field at a time (typical of the horizontal resolution of radio occultation measurements which is of the order of 300 km), the complete field was traversed. Computing the ensemble mean from the difference between the two versions of the forward models allowed a reasonable estimate of the forward modelling error incurred by the spherical symmetry assumption to be computed. It is noted that this error estimate does not represent the true error in observation space since the forward model does not simulate the full error characterisation. Both *Ahmad and Tyler*, [1999] and *Healy*, [1999] consider bending angle errors from horizontal gradients for specific cases. However there is no published material that quantifies this error statistically. Simulation with a full 3-d raytracer through the UKMO mesoscale model fields suggest that the errors are approximately 3% for ray paths near the surface, which is consistent with the value used in this work.

An error arises from representing an intrinsically high resolution problem with a crude resolution. This type of error is often called a representativeness error and describes the error from the inability of NWP model vertical grids to represent small-scale atmospheric structure, which are evident in GPS/MET RO measurements [*Kursinski et al*, [1997]]. The method used to estimate this quantity is described by *Healy*, [1998], and is found to be of the order of 2% of the bending angle measurement in the troposphere and upper stratosphere, decreasing slightly in the middle stratosphere. This variation in the error is associated with the temperature variations in these region.

The forward model used is based on geometric optics therefore does not account for atmospheric diffraction. However, *Kursinski et al*, [1997] have shown that the geometric optics assumption is successful in describing propagation characteristics above a certain diffraction limit, and diffraction is therefore not considered here.

Forward model parameter errors Uncertainties associated with the physical constants used to model the physical system also cause modelling errors. The major physical constants used in the forward model are the refractivity coefficients (c_1 and c_2

in equation 8) and the local radius of curvature.

The uncertainty of the refractivity coefficients do not represent the error associated with their values but the uncertainty of the measured quantity; for this reason the information will not be included in the total observation error budget since it will result in a bias in the retrieval⁶. The local radius of curvature assumed for zero altitude is a parameter that is used to compute the bending angle observations from atmospheric phase delay, therefore any error associated with this parameter will be present in the bending angle observations. This parameter is also used to compute geometric height levels from impact parameter levels. The uncertainty of this value is estimated to be approximately 100 metres [*Kursinski et al*, [1997]].

Total observation error The total observation error covariance \mathbf{E} is constructed by adding the covariance matrices from observation noise, forward modelling and forward model parameters.

The diagonal terms have also been constrained not to fall below a minimum value to account for the noisy upper stratosphere measurements.

Figure 3 shows how the standard deviation values of the principal diagonal from each error contribute to the observation error covariance matrix.

The dominant source of error for the majority of the vertical range considered is the forward modelling error, i.e. representativeness error and horizontal inhomogeneity error, with the upper stratospheric noise limit providing the second largest contribution to the total error. In the upper stratosphere the total bending angle reverts to the upper level minimum noise used. At near-surface altitudes, the forward model parameter error, i.e. local radius of curvature, is significant. The overall effect from the local radius of curvature decreases exponentially due to the hydrostatic relation.

3.3. Convergence and quality control

The method used to judge convergence relies upon values of the cost function, i.e. if the relative change is smaller than a specified value (0.5%) then the solution is determined to have converged. This method alone is found to be a good indicator of convergence in this case.

For the work presented in this paper, the maximum number of iterations considered is 10; if the so-

⁶Optimal estimation theory assumes that all the errors are unbiased.

lution has not converged (determined by the method presented above within 10 iterations) then the calculation is halted and a numerical ‘flag’ set.

If, after convergence has been determined, the $\mathbf{J}(\mathbf{x})$ value is greater than the χ^2 value given the number of degrees of freedom at a set confidence level (in this case 99.9%) then a numerical ‘flag’ is set. Retrievals with flags set are omitted from any statistics.

Furthermore, to ensure the solution computed at each iteration is physical, the $\ln(\text{specific humidity})$ elements are checked for super-saturation and corrected if necessary.

4. Results

In this section the performance of the optimal estimation retrieval scheme is examined using simulated profiles and realistic error estimates. For each simulated profile, a ‘true’ profile is established by taking one of a set of profiles of UKMO model analyses from which to compute the ‘true’ observation vector. The associated background atmospheric profile is calculated by perturbing the ‘true’ profile thus

$$\mathbf{x}^b = \mathbf{x}^t + \sum_{i=1}^n \epsilon_i \lambda_i^{1/2} \mathbf{P}_i \quad (12)$$

where the superscript t denotes the ‘truth’, λ_i and \mathbf{P}_i are the i th eigenvalues and eigenvectors of the forecast error covariance matrix and ϵ_i represents the i th number drawn from a normal distribution of random numbers.

Observation noise is modelled and superimposed onto the observation vector using the method analogous to equation 12, utilising the eigenvector and eigenvalues from the total observation error covariance matrix.

4.1. Ensemble of numerical simulations

Using the method described by equation 12, simulated observations and realistic background profiles were produced. These were used as inputs to the inversion scheme to obtain retrieved profiles which were subsequently compared with the ‘true’ profiles to assess the impact of the observations on the background information.

The observation level values (i.e. impact parameter, local radius of curvature and geographical position) have been taken from data during ‘prime-times’⁷

1 and 2 [Rocken *et al*, 1997], in an effort to simulate realistic retrieval scenarios. The latitudinal and longitudinal distribution of these occultation events (determined by GPS sampling) are varied, thus providing a mixed ensemble of polar, tropical and mid-latitudinal occultation events.

Five hundred profiles with random temperature, humidity and surface pressure conditions have been tested, and successful retrievals (i.e. which pass quality control) were obtained in all but eight cases. In most cases convergence is obtained within three or four iterations. In general, the $\mathbf{J}(\mathbf{x})$ values at convergence were comparable to the number of degrees of freedom considered, as expected [Marks and Rodgers, 1993]. This suggests that although the χ^2 quantity is only strictly valid for linear problems it can be used reliably as a quality control for the retrieval.

The eight cases which do not pass the specified quality control have been examined. They are found to be cases in which the cost function has been minimised successfully but the converged value is too large compared with the χ^2 distribution. These spurious converged profiles represent artificial outliers, which are generated when the increment described by equation 12 is large enough to make the inverse problem grossly non-linear. A small number of profiles are expected to have this problem due to the normal distribution of random numbers used in the method of simulating atmospheric profiles. The profiles which failed the quality control have not been included in the statistics shown.

For each successful retrieval, the retrieval error and the background error (first-guess error) have been calculated, and the mean and standard deviation values of these data have been computed. The standard deviation values represent the errors ascribed to each element of the solution and background state vector, and can be compared directly with the square root values of the principal diagonal of the background error covariance matrix assumed in the retrieval. The ratio of the retrieval error estimates to the forecast error estimates is related to the amount of information the measurements supply to the NWP system.

An improvement vector is defined which indicates how the retrieval has improved the knowledge of the background state throughout the atmospheric profile, and will be used to complement the r.m.s. statistics presented. The improvement vector $\boldsymbol{\eta}$ is given by

anti-spoofing military encryption.

⁷Periods of time when the received signals are free from

$$\eta_j = 100 \times \left[1 - \left(\frac{\hat{\mathbf{S}}_{j,j}}{\mathbf{C}_{j,j}} \right)^{\frac{1}{2}} \right] \quad (13)$$

where j is the matrix and improvement vector element index, and all other variables are as before.

The results from the ensemble of simulated retrievals are summarised by figure 4. The upper panels ((a) and (b)) show the computed r.m.s. errors from the the simulated retrievals. The forecast errors resemble those shown by figure 2 as expected, modified slightly by the modelled observation noise.

The temperature improvement vector suggests that optimal estimation considerably improves upon the prior knowledge of the atmospheric temperature, from the lower-troposphere to the mid-stratosphere. The temperature improvement vector declines in the upper stratosphere partly because of the upper noise limit used, which is comparable to forecast errors in observation space, and partly because it represents the lower limit of the observation vectors used in the ensemble of simulations. The temperature improvement vector declines in the lower-troposphere where humidity becomes more significant, and both quantities are retrieved simultaneously, thus the emphasis is shifted from temperature to $\ln(\text{specific humidity})$. It is clear from the plot that there is a gradual decline in the temperature retrieval quality from 300 to 1000 hPa as the humidity retrieval quality improves, where the background uncertainty information is being used to resolve the temperature-specific humidity ambiguity in the refractivity.

Both the temperature and humidity knowledge decline near the surface because the majority of occultation events presented here terminate typically above one kilometre.

The results shown by figure 4 confirm that the method is suitable for the purpose of non-linear optimal estimation using RO measurements. Together, the theoretical r.m.s. errors and the computed improvement vectors suggest that there are improvements in the prior knowledge of the atmospheric state from near-surface to the upper stratosphere. In particular, the level of surface pressure improvement suggests that the RO observations can improve the prior knowledge of the surface pressure.

4.2. Solution error characterisation

Using the optimal estimation inverse theory outlined in section 3 an error analysis can be obtained

which allows a full characterisation of the solution (for a detailed account see *Rodgers, [1990]*). The error associated with the solution vector can be split into its constituent parts, namely error from the background error estimates, forward modelling, forward model parameters and observation noise. A mid-latitude retrieval⁸ (which spans 0.7–60 km) has been used as an example to illustrate the method (figure 5).

Panels (a) and (b) show that the *a priori* provides almost all the information to the temperature and $\ln(\text{specific humidity})$ retrieval above 10 hPa and 500 hPa, respectively.

Panels (c) and (d) show the observation noise contribution to the retrieval error which is comparatively small.

Panels (e) and (f) show the forward modelling contribution to the retrieval error. The structure of this contribution is very similar to that of the observation noise, but has a larger associated error. In general, forward modelling represents the second largest contribution to retrieval error.

The temperature solution error contributions shown by panels (c) and (e) peak at 3 hPa, at the point where the stratospheric noise limit contribution to the total observation error budget peaks (figure 3). The observation contribution to the solution error begins to increase above about 0.3 hPa. Above this pressure level the *a priori* increases more rapidly, and so the observation is given more weight, resulting in a larger contribution to the solution error.

Panels (g) and (h) show that forward model parameter error represents the smallest contribution to the total retrieval error. This contribution to the temperature and $\ln(\text{specific humidity})$ solutions peak near 1000 hPa due to the local radius of curvature error. The contribution to the surface pressure solution represents a small fraction of the total retrieval error.

Figure 5 indicates that the dominant contributions to the solution error are from the *a priori* and forward modelling, suggesting that particular efforts should be made to improve their accuracies. It should be noted that the solution error depends on the assumptions made about the uncertainty statistics.

4.3. Quality of surface pressure retrievals

It is found that the quality of the surface pressure retrievals is dependent on the vertical extent of

⁸Henceforth will be referred to as the example occultation profile.

the occultation, i.e. how closely it approaches the surface. To illustrate this point, the example occultation profile is used. By systematically removing observations near the surface and re-retrieving temperature, $\ln(\text{specific humidity})$ and surface pressure, it can be shown how the vertical range of the occultation is important to the quality of the surface pressure retrieval (figure 6).

Panels (a), (b) and (c) show the temperature, $\ln(\text{specific humidity})$ and surface pressure improvement vectors get smaller in the lower atmosphere with increasing values for the lowest geometric height level, as expected. Panel (d) shows that the retrieval which includes all the observations provides enough information to retrieve accurately the true value for surface pressure; as the number of near-surface observations decreases the retrieval becomes smaller and smaller, approaching the prior value.

It is interesting to note that the surface pressure information does not decrease as quickly as expected. Indeed there is still a considerable amount of surface pressure information towards the upper troposphere. This variation in surface pressure information is due to the link between height and pressure through the hydrostatic relation.

It can be concluded from this experiment that using optimal estimation, radio occultation measurements of the Earth possess surface pressure information even if the occultation has been completed in the mid-troposphere (e.g. due to atmospheric multipath interrupting the transmitted signal). This is important to appreciate when validating surface pressure retrievals using real data.

4.4. Sensitivity to inverse model statistics

In this section we present the results from a sensitivity study in which the statistics used to compute the optimal estimate are changed in order to investigate the retrieval sensitivity to such alterations. The three statistics that are altered are the observation noise, the forward modelling error and the forecast error since these represent the largest contributions to the solution error as shown by figure 5.

Altering the observation noise may simulate the possible changes in observation noise sources, e.g. improved high-order ionospheric or poor quality clocks aboard the GPS receivers.

Changing the forward modelling error is a crude method of simulating the possibility of assimilating intrinsically high resolution GPS radio occultation

measurements with lower or higher resolution NWP model fields, and/or an occultation through a frontal system or a relatively horizontally inhomogeneous atmosphere.

Altering the prior error covariance matrix represents the effect of changing the prior knowledge of the atmosphere. Increasing these error estimates can represent the extent of the knowledge of the atmosphere in the southern hemisphere where other atmospheric information is sparse. Decreasing this error may represent a more realistic model dynamics/climatology and/or greater confidence in other similar atmospheric observations used to initialise the model. For this particular test the variance values are changed, whilst retaining the existing correlations.

Figure 7 shows the improvement vectors from the retrieval sensitivities outlined above. Improvement vectors are used to present the results of this study because it is the relative improvement on the prior estimate of the atmospheric state that we are interested in.

Panels (a) and (b) shows that doubling or halving the observation noise has little effect on the overall improvement, reflecting the contribution from this error source to the total observation error covariance matrix (figure 3). The changes due to $\ln(\text{specific humidity})$ are very slight. The surface pressure improvement changes typically by a few percent.

Panels (c) and (d) correspond to increasing or decreasing the forward modelling error (by 50%). This error source provides the largest contribution to the total observation error, and as such has a large influence on the degree of improvement. The difference in the temperature improvement is of the order of 15% in the upper troposphere and lower stratosphere, above which other error sources are more important, and below which (the lower troposphere) the emphasis is shifted from the temperature retrieval to the $\ln(\text{specific humidity})$ and surface pressure retrieval. The improvement response for $\ln(\text{specific humidity})$ is less pronounced than for temperature peaking at $\pm 8\%$. The surface pressure improvement variation is approximately $\pm 15\%$.

Panels (e) and (f) shows that increasing or decreasing the standard deviation of the prior error increases or decreases the improvement of temperature, $\ln(\text{specific humidity})$ throughout the vertical range of the observations as expected. Decreasing the *a priori* error means better background knowledge, consequently the weighting of the *a priori*/observation is increased/decreased. This corresponds to a small

improvement relative to the background atmospheric knowledge. Positive and negative temperature improvement differences are of the order of 20% throughout the range described by the observation vector; the $\ln(\text{specific humidity})$ improvement is of the order of $\pm 10\%$; and the surface pressure improvement is of the order of $\pm 10\%$.

This sensitivity study has looked at some of the extreme case scenarios in which the statistics assumed for the optimal estimation inverse method have been changed. It has been shown that the retrieval method is most sensitive to the background errors and forward modelling errors; the latter being related to errors due to the spherical symmetry assumption. The results from increasing the background error estimates are especially important to note since they represent a real possibility when dealing with any reasonable measurements in the data sparse southern hemisphere.

5. Conclusions

In this paper we have demonstrated a prototype optimal estimation inverse method for GPS radio occultation observations.

The method is a non-linear, maximum *a posteriori* technique which can accommodate most aspects of the real radio occultation problem. In particular, it is able to account for some of the error incurred from assuming local spherical symmetry which is not possible using the analytic inverse method. The optimal estimation technique handles the temperature–water vapour ambiguity in a more rigorous way, rather than the sub-optimal manner inherent with the analytic inverse method.

The optimal estimation inverse method is used here as an iterative method but is found to be stable and to converge rapidly in most cases. The value of the cost function at each iteration can be used reliably to judge convergence and as an indicator of sensible results, allowing anomalous retrieval conditions to be recognised and omitted, thus preventing gross retrieval errors.

The method is shown to be suitable for retrieving values for surface pressure. Hence, this method of utilising radio occultation observations of the Earth's atmosphere has the potential to improve both atmospheric and oceanographic models, which may lead to improved predictions of the weather and climate. The quality of the surface pressure retrieval is shown to depend on the vertical extent of the occultation, i.e. higher quality retrievals are attainable with oc-

cultations that reach low altitudes.

It should be noted that the background statistics assumed in the paper represent global statistics. However, for purposes of demonstrating a prototype retrieval scheme for radio occultation observations they are found to be adequate. It has been shown that the retrieval accuracies, and hence the weight which should be given to the data in the subsequent model analysis, are sensitive to both forecast error uncertainties and values used to describe the forward modelling error.

Acknowledgments. The authors would like to thank the Jet Propulsion Laboratory for providing the GPS/MET radio occultation dataset, J. P. Luntama for the bending angle error estimates, and C. D. Rodgers, A. Dudhia and H. Roscoe for comments on earlier drafts.

References

- B. Ahmad and G. L. Tyler, Systematic errors in atmospheric profiles obtained from Abelian inversion of radio occultation data: Effects of large-scale horizontal gradients, *J. Geophys. Res.*, *104*, 3971-3992, 1999.
- M. Born and E. Wolf, Principles of Optics, *Pergamon Press*, 1993.
- Cospar International Reference Atmosphere: 1986. Part II: Middle Atmosphere Models, *Adv. Space Res.*, *10*, 1990.
- M. P. Cullen, The unified forecast/climate model, *Met. Mag.* *112*, 1449-1451, 1993.
- J. R. Eyre, Inversion of cloudy satellite sounding radiances by nonlinear optimal estimation. I: Theory and simulation for TOVS, *Q. J. R. Meteorol. Soc.*, *116*, 401-434, 1989.
- J. R. Eyre, Assimilation of Radio Occultation Measurements into a Numerical Prediction System, ECMWF Tech. Memo No 199, 1994.
- G. Fjeldbo and V. R. Eshleman, The Atmosphere of Mars Analysed by Integral Inversion of the Mariner IV Occultation Data, *Planet Space Science*, 1035-1059, 1968.
- G. Fjeldbo and A. J. Kliore, The Neutral Atmosphere of Venus as Studied with the Mariner V Radio Occultation Experiments, *The Astronomical Journal*, *76*, 123-139, 1971.
- A. S. Gurvich and T. G. Krasil'nikova, Navigation satellites for radio sensing of the Earth's atmosphere, *Sov. J. Remote Sensing*, *7*, 1124-1131, 1990.
- S. B. Healy, A statistical comparison of GPS/MET radio occultation data with numerical weather prediction analyses, UKMO Tech. Memo No. 247, 1998.
- S. B. Healy and J. R. Eyre, Retrieving temperature, water vapour and surface pressure information from refractive index profiles derived by radio occultation: a simulation study, accepted by *Q. J. R. Meteorol. Soc.*

- S. B. Healy, Radio occultation bending angle errors caused by horizontal gradients: a simulation study, UKMO Tech. Memo No. 286, 1999. (also submitted to *J. Geophys. Res.*, 1999).
- A. J. Kliore, G. Fjeldbo, B. L. Seidel, D. N. Sweetham, T. T. Sesplaukis, P. M. Woiceshyn and S.I. Rasool, The Atmosphere of Io from Pioneer 10 Radio Occultation Measurements, *Icarus*, *24*, 407-410, 1975.
- Y. H. Kuo, X. Zou and W. Huang, The impact of Global Positioning System data on the prediction of an extratropical cyclone: an observing system simulation experiment, *J. Dyn. Atmos. Ocean*, *27*, 439-470, 1998.
- E. R. Kursinski, G. A. Hajj, W. I. Bertinger, S. S. Leroy, T. K. Meehan, L. J. Romans, J. T. Schofield, D. J. McCleese, W. G. Melbourne, C. L. Thornton, T. P. Yunck, J. R. Eyre and R. N. Nagatani, Initial Results of Radio Occultation of Earth's Atmosphere using GPS, *Science*, *271*, 1107-1110, 1996.
- E. R. Kursinski, G. A. Hajj, K. R. Hardy, J. T. Schofield and R. Linfield, Observing the Earth's Atmosphere with Radio Occultation Measurements using GPS, *J. Geophys. Res.*, *102*, D19, 23429-23465, 1997.
- G. F. Lindal, G. L. Sweetham and V. R. Eshleman, The Atmosphere of Saturn: An Analysis of the Voyager Radio Occultation Measurements, *Astron. J.*, 1136-1146, 1985.
- G. F. Lindal, J. R. Lyons, G. L. Sweetham, V. R. Eshleman, D. P. Hinson and G. L. Tyler, The Atmosphere of Uranus: Results of Radio Occultation Measurements with Voyager 2, *Geophys. Res. Lett.*, 14987-15001, 1987.
- G. F. Lindal, The Atmosphere of Neptune: An Analysis of Radio Occultation Data Acquired with Voyager 2, *Astron. J.*, *103*, 967-982, 1992.
- A. C. Lorenc, Analysis method for numerical weather prediction, *Q. J. R. Meteorol. Soc.*, *112*, 1177-1194.
- J. P. Luntama, Atmospheric Profiling with Radio Occultation, Master's Thesis, Department of Electrical and Communications Engineering, Helsinki University of Technology, Finland, 1997.
- C. J. Marks and C. D. Rodgers, A Retrieval Method for Atmospheric Composition from Limb Emission Measurements, *J. Geophys. Res.*, *98*, D8, 14939-14953, 1993.
- M. D. Mortensen and P. Høeg, Inversion of GPS occultation measurements using diffraction theory, *Geophys. Res. Lett.*, *25*, 13, 2441-2444, 1998.
- P. I. Palmer, Analysis of atmospheric temperature and humidity from radio occultation measurements, D.Phil. thesis, Oxford University, 1998.
- R. A. Phinney and D. L. Anderson, On the Radio Occultation Method for Studying Planetary Atmospheres, *J. Geophys. Res.*, *73*, 1819-1827, 1968.
- W. H. Press, S. A. Teukolsky, W. T. Vetterling and B. P. Flannery, Numerical Recipes in FORTRAN: The art of scientific computing, Cambridge Univ. Press, 1992.
- C. Rocken, R. Anthes, M. Exner, D. Hunt, S. Sokolovskiy, R. Ware, M. Gorbunov, W. Shreiner, D. Feng, B. Herman, Y.-H. Kuo and X. Zou, Analysis and validation of GPS/MET data in the neutral atmosphere, *J. Geophys. Res.*, *102*, D25, 29849-29866, 1997.
- C. D. Rodgers, Retrieval of Atmospheric Temperature and Composition from Remote Measurements of Thermal Radiation, *Rev. Geophys.*, *14*, 609-624, 1976.
- C. D. Rodgers, Characterization and Error Analysis of Profiles Retrieved from Remote Sounding Measurements, *J. Geophys. Res.*, *95*, D5, 5587-5595, 1990.
- E. K. Smith and S. Weintraub, The constants in the equation for atmospheric refractive index at radio frequencies, *Proc. of the I.R.E.*, *41*, 1053-1037, 1953.
- A. K. Steiner, G. Kirchengast and H. P. Ladreiter, Inversion error analysis, and validation of GPS/MET occultation data, *Ann. Geophysicae*, *17*, 122-138, 1999.
- S. Syndergaard, Retrieval analysis and methodologies in atmospheric limb sounding using the GNSS radio occultation technique, Ph.D. thesis, DMI Scientific Report, 99-6, Danish Meteorological Institute, Copenhagen, 1999.
- R. Ware, M. Exner, D. Feng, M. Gorbunov, K. Hardy, W. Melbourne, C. Rocken, W. Schreiner, S. Sokolovskiy, F. Solheim, X. Zou, R. Anthes, S. Businger and K. Trenberth, GPS Sounding of the Atmosphere from Low-Earth Orbit: Preliminary Results, *Bull. Am. Meteorol. Soc.*, 19-40, 1996.
- V. V. Vorob'ev and T. G. Krasil'nikova, Estimation of the Accuracy of the Atmospheric Refractive Index Recovery from Doppler Shift Measurements at Frequencies Used in the NAVSTAR System, USSR Physics of the Atmosphere and Ocean (Engl. Transl.), *29*, 5, 602-609, 1994.
- X. Zou, Y. H. Kuo and Y. R. Guo, Assimilation of Atmospheric Radio Refractivity Using a Nonhydrostatic Adjoint Model, *Mon. Weather Rev.*, *123*, 2229-2249, 1995.

Dr. Paul I. Palmer, Division of Engineering & Applied Science, Pierce Hall, Harvard University, Cambridge, MA 02138 (e-mail: pip@io.harvard.edu)

Received August, 1999; revised January, 2000; accepted February, 2000.

¹Now at Division of Engineering & Applied Science, Pierce Hall, Harvard University, Cambridge, MA 02138

This preprint was prepared with AGU's L^AT_EX macros v5.01. File gpsinverse formatted December 23, 2021.

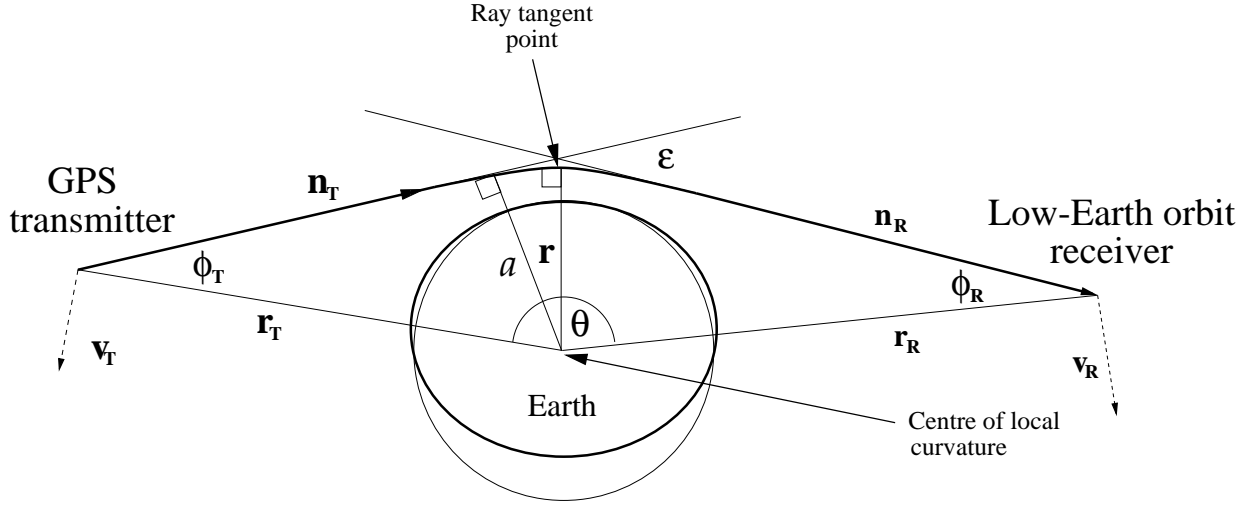


Figure 1. Defining the radio occultation geometry used to obtain bending angle information from the time delay caused by the Earth’s atmosphere. A tangential sphere is superimposed on to the oblate Earth (exaggerated) to emphasise the position of the local radius of curvature at the ray periapsis. The dashed lines indicate motion.

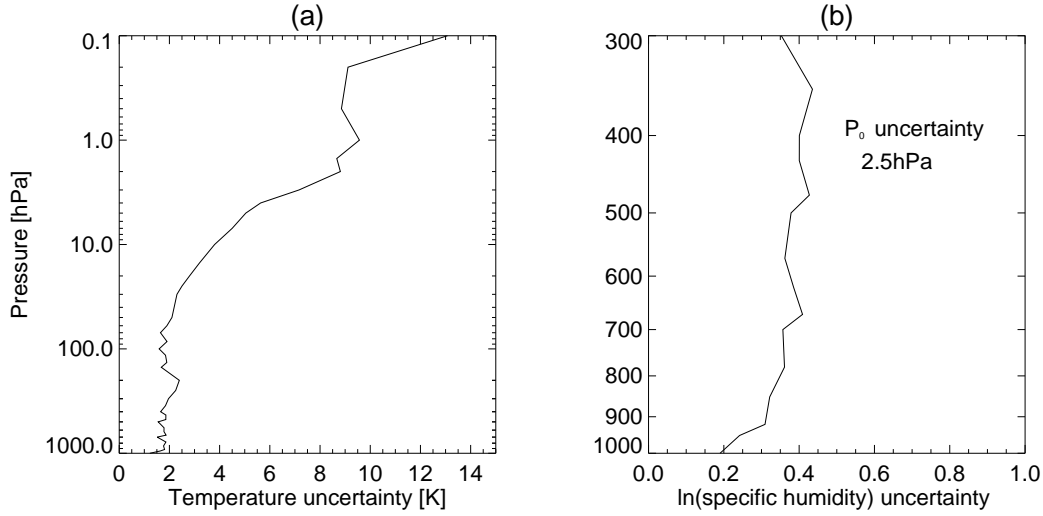


Figure 2. The square-root values of the principal diagonal of the UKMO forecast error covariance matrix. Panels (a) and (b) show the assumed uncertainty for prior temperature and $\ln(\text{specific humidity})$, respectively, with the assumed prior uncertainty for the surface pressure element inset of panel (b).

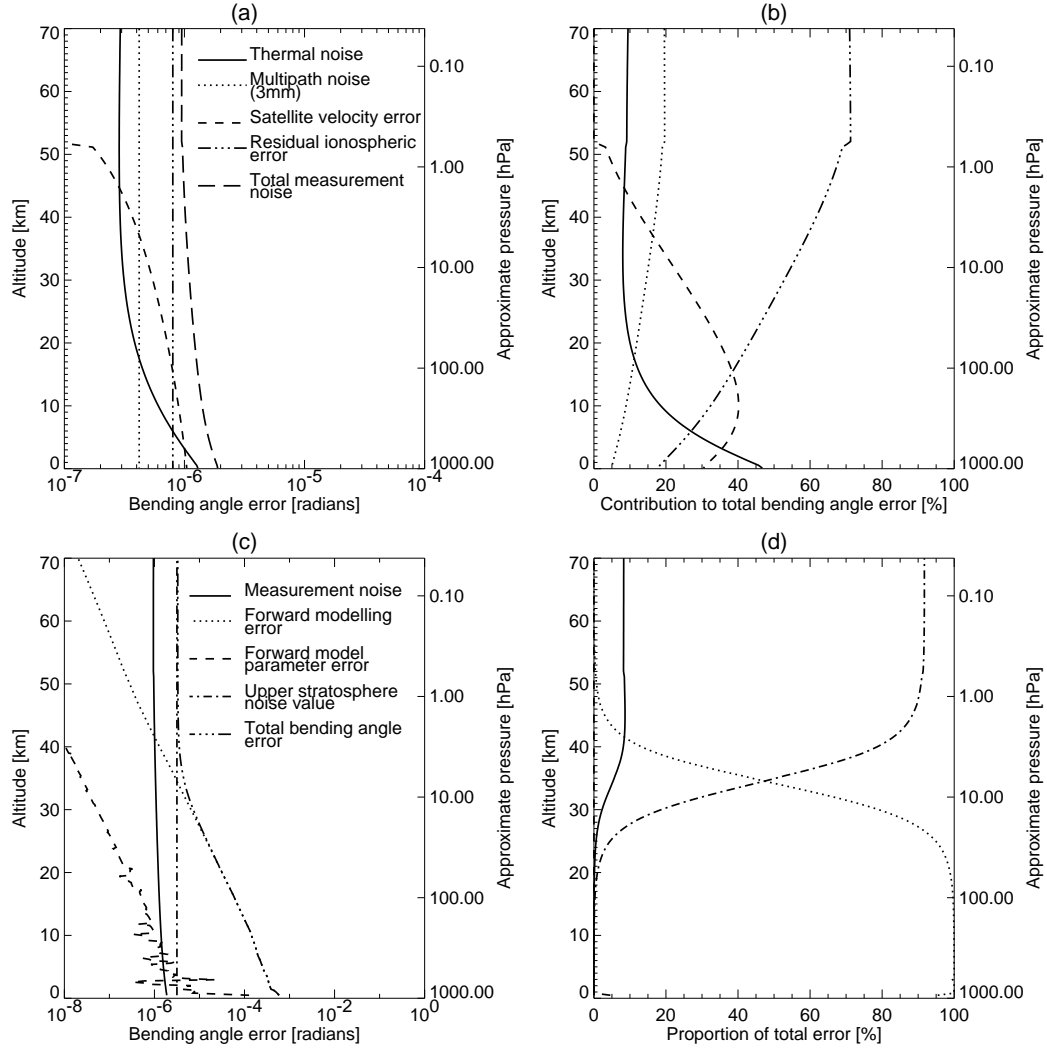


Figure 3. Measurement noise budget and total measurement error budget for the RO optimal estimation inverse method [after Luntama, [1997]]. The error estimates shown in panel (a) represent normal atmospheric conditions, i.e. small multipath error (3 mm) and normal ionospheric conditions. Panel (b) shows the percentage contributions from the different error sources to the total bending angle error. Panel (c) shows typical standard deviation values from the principal diagonal from each contribution to the total measurement error covariance matrix; and panel (d) shows the individual measurement error sources as a percentage proportion of the total error.

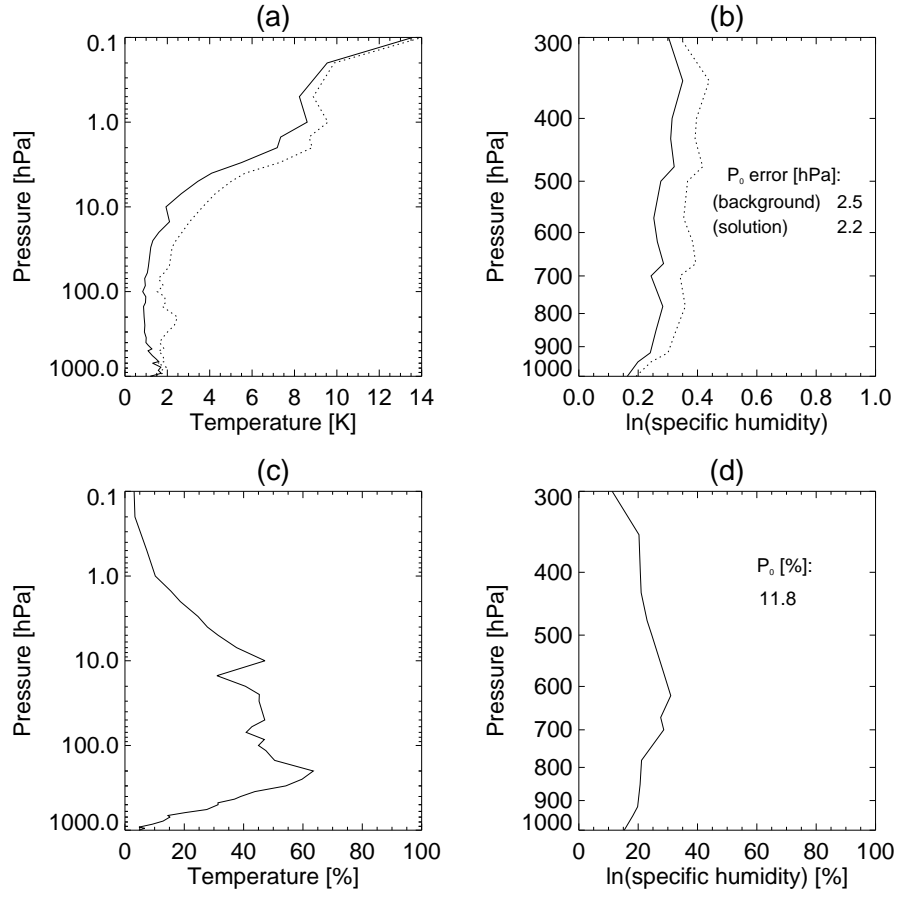


Figure 4. Theoretical error estimates from the ensemble of simulated retrievals. The upper panels show the theoretical r.m.s errors, where the solid and dotted lines represent the retrieval and background errors, respectively. Panel (a) shows the errors from the temperature solution and the panel (b) shows the errors from the $\ln(\text{specific humidity})$ solution with the surface pressure solution error inset. The lower panel show the corresponding improvement vector. Panels (c) and (d) show the temperature and $\ln(\text{specific humidity})$ elements with the surface pressure improvement inset of panel (d).

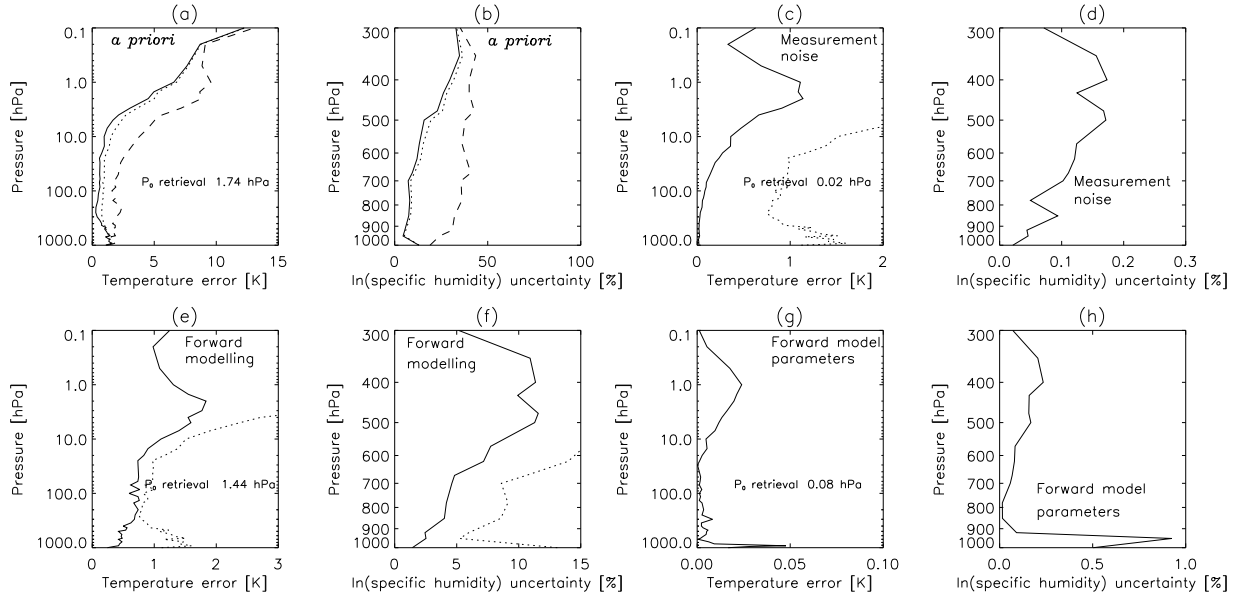


Figure 5. Solution error characterisation of the optimal estimation inverse method for the example occultation profile. Left panels of a pair show the contribution to the temperature retrieval error and the right panels show the error contributions to the $\ln(\text{specific humidity})$ retrieval error. The surface pressure retrieval error is inset of the left panels. Panels (a) and (b) show the *a priori* contribution to the retrieval error, where the dashed shown represent the standard deviation values of the principal diagonal of the *a priori* error covariance matrix; (c) and (d) the measurement noise contribution; (e) and (f) the forward modelling contribution; and (g) and (h) the forward model parameter contribution. The total solution error is superimposed on all panels (dotted line) to provide an indication as to which contributions are prominent.

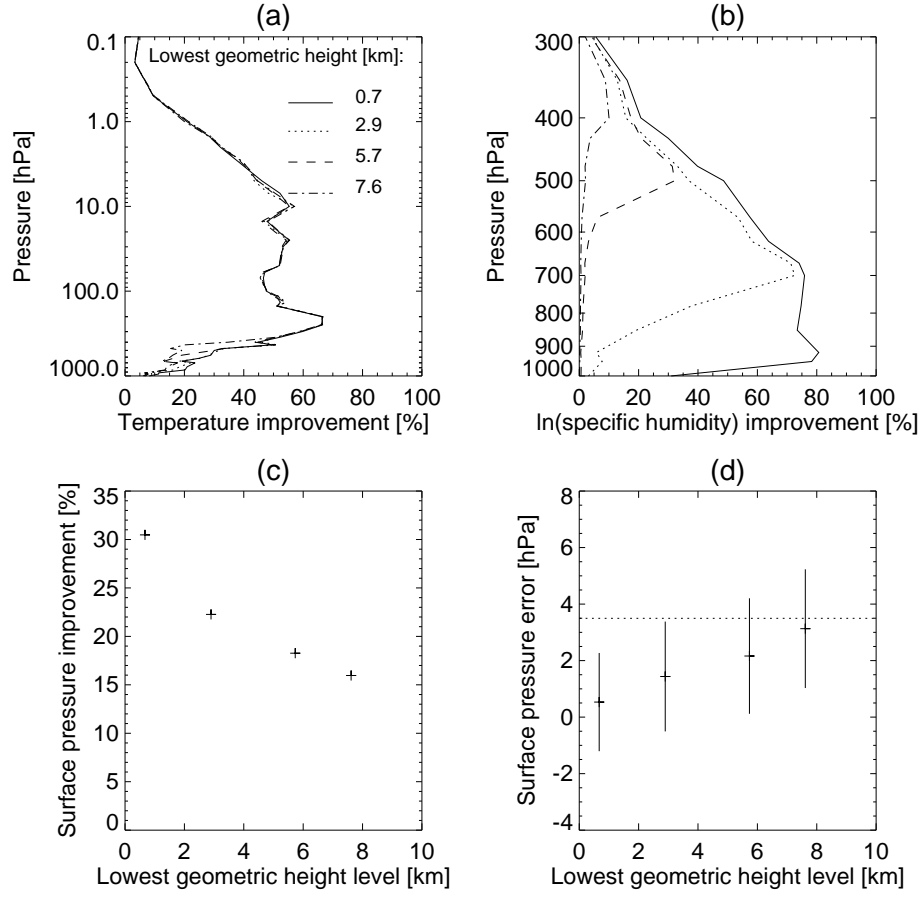


Figure 6. Investigating the relationship between the quality of surface pressure retrievals and the lowest geometric height level of the occultation using the example occultation profile. Panel (a), (b) and (c) show the temperature, $\ln(\text{specific humidity})$ and surface pressure improvement vectors; and panel (d) shows the difference (with errors bars) between the truth and the retrieval. The broken line in panel (d) represents the difference between the ‘true’ and the assumed value for the surface pressure.

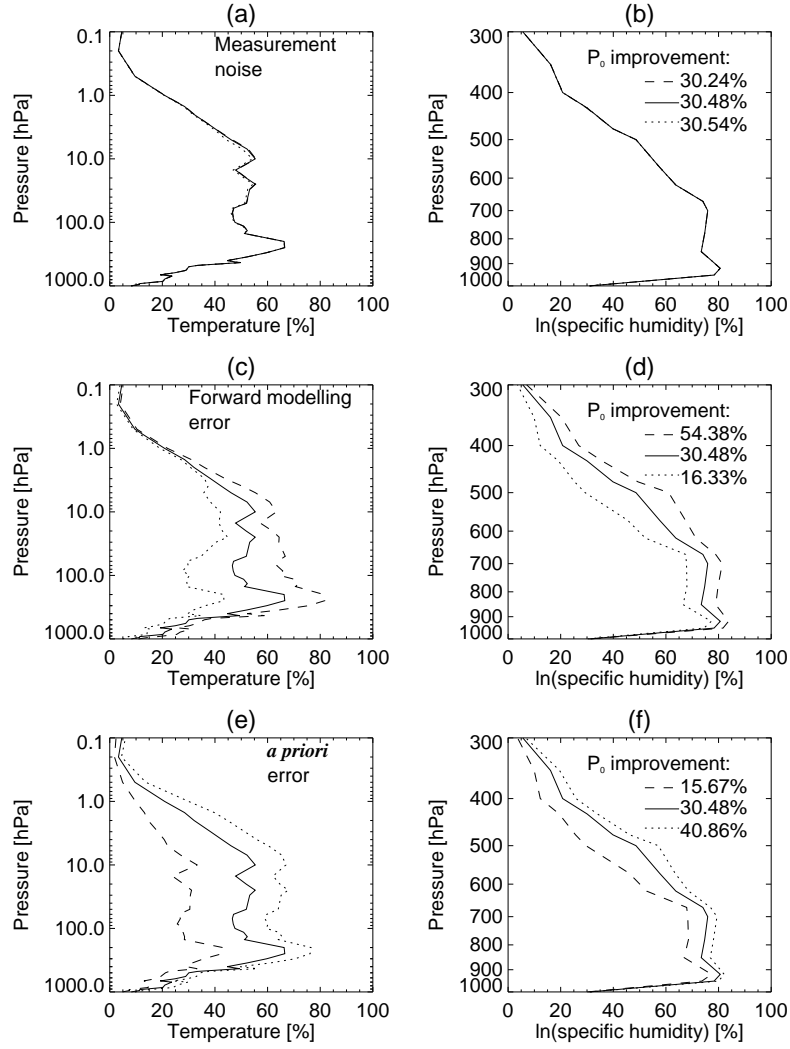


Figure 7. Improvement vectors from the retrieval sensitivity studies using the example occultation profile. In general, left panels show the temperature improvement vector elements and the right panels show the $\ln(\text{specific humidity})$ improvement vector elements, with the surface pressure improvement vector element inset. For panels (a)–(f), dashed curves represent a reduction in the quantity altered, dotted curves represent an increase in the quantity altered and solid curves represent the control case. Panels (a) and (b) show the results from doubling/halving the measurement noise; panels (c) and (d) show the results from increasing and decreasing the representative error by $\pm 50\%$; and panels (e) and (f) show the results from increasing and decreasing the principal diagonal standard deviation errors from the *a priori* error covariance matrix by $\pm 50\%$.